Enhancements of pinning by superconducting nanoarrays

E. Navarro,[1,2] C. Monton,[1] J. Pereiro,[1,3] Ali C. Basaran,[1,4] and Ivan K. Schuller[1]

[1]*Department of Physics and Center for Advanced Nanoscience, University of California San Diego, La Jolla, California 92093, USA*
[2]*Departamento de Física de Materiales, Facultad de Físicas, Universidad Complutense, 28040 Madrid, Spain*
[3]*School of Physics and Astronomy, Cardiff University, The Parade, Cardiff CF24 3AA, United Kingdom*
[4]*Department of Physics, Gebze Technical University, Gebze, Kocaeli 41400, Turkey*

We present a comparative study of vortex pinning efficiency in superconducting (V) thin films grown on two similar triangular arrays of superconducting (Nb) and nonsuperconducting (Cu) nanodots. Resistance and magnetization anomalies at the same matching fields confirm the same pinning periodicity in both samples. However, we found two distinct features: First, the sample with superconducting dots shows stronger pinning that appears as sharper matching peaks in magnetization loops and shows higher critical current density and larger critical field at low temperatures. Second, an overall increase in the resistance of the V film with Nb nanodots is observed, while there is a crossover in the temperature dependence of the critical field and the critical current of both samples at $T = 3$ K. This crossover corresponds to the temperature when the superconducting coherence length of V thin film equals the edge-to-edge distance between nanodots. We argue that this change in superconducting properties is related to the change in the superconducting regime from pinning enhancement at low temperatures to a superconducting wire network at high temperatures.

I. INTRODUCTION

The improvement of vortex pinning efficiency in type-II superconductors has been the focus of many experimental and theoretical investigations [1]. It is well established that artificial pinning centers can substantially enhance the superconducting critical current density (J_C) whenever the density of vortices matches the underlying pinning landscape ("pinning enhancement"). This commensurability effect between vortices and pinning landscape has been widely studied in different periodic [2] and nonperiodic [3,4] pinning geometries using pinning centers such as micrometric and submicrometric holes [5–8], blind holes [9,10], and magnetic [11,12] and nonmagnetic dots [13,14].

Matching effects appear as "dips" in the magnetic field dependence of the resistance, $R(H)$, and "peaks" in the field dependence of the magnetization, $M(H)$, when an integer number of flux quanta, $n\phi_o$, is commensurate with the unit cell of the pinning centers [5]. However, when the width (w) of the superconducting (SC) strips around the dots is comparable to the SC coherence length, $\xi(T)$, the vortices are too large to locate in interstitial positions. In this case, matching also occurs at integer flux quantum fields, but the sample is described as a SC wire network [15]. These matching effects are due to the additional suppression of the SC critical temperature (T_C) by magnetic field at noninteger flux quantum values arising from the fluxoid quantization, the so-called Little-Parks effect [16,17].

It has been theoretically demonstrated that a stable vortex configuration can be achieved using a SC pinning landscape [18]. In this case, SC dots contribute to the pinning through two mechanisms: (i) structural defects due to the corrugation and (ii) diamagnetic contribution of the dots in the SC state. The latter distinguishes the pinning mechanisms of SC pinning centers from normal or magnetic pinning centers. However, little experimental work has been done in exploring SC pinning landscapes [19,20]. In Ref. [19] periodic square arrays of Nb cylinders were used as pinning centers for Nb. These SC pinning centers are found to be repulsive for the SC vortices. While these studies did not observe clear matching resistance minima, the slope of $R(H)$ changed at matching fields, i.e., where the number of vortices was an integer or half integer times the number of protruding cylinders. Subsequent work reported [20] on the vortex dynamics of Nb thin films containing a dense triangular array of submicron V dots, in which the T_C (Nb film) was larger than the T_C (V dots). In this case, the ac susceptibility shows an abrupt change in vortex mobility across the expected superconducting transition of the V dots. The vortex lattice responds with lower mobility when the V dots are in the SC state. Due to the low superconducting critical field of the V dots, this behavior could only be observed in a limited field region. While these works show the pinning properties of SC dots and suggest the possibility of commensurability effects by a SC pinning landscape, they do not probe the pinning strength nor do they provide direct evidence of the superconducting character of the dots. We propose an approach in which the T_C of the SC film is lower than the T_C of the pinning centers which allows investigating the effectiveness of pinning landscape in a wider range of temperature and applied fields.

In this work we present a study on superconducting V films with periodic superconducting Nb nanodot arrays, in which the pinning centers have higher T_C than the SC film. We observe clear commensurability effects due to SC pinning and we compare it with an equivalent sample with nonsuperconducting (Cu) nanodots. We show that Nb pinning centers are more effective than Cu pinning centers, with ~30% higher critical current density (J_C) at low temperatures. However, the temperature dependence of the superconducting

properties of the V film is unexpected. The critical field (H_{C2}) and J_C of V on SC dots drop below the values of V on nonsuperconducting dots at $T > 3$ K. We relate this decrease to the crossover between the coherence length [$\xi(T)$] and the edge-to-edge separation between the dots.

II. EXPERIMENTAL DETAILS

We compared the properties of three different samples: (1) "Nb-down," consisting of an array of superconducting Nb dots with a V film on top; (2) "Cu-down," consisting of an array of nonsuperconducting Cu dots with a V film on top; and (3) "Nb-up," consisting of an array of Nb dots deposited directly on top of a V film. Samples (1) and (2) which are corrugated due to the underlying dots were used to study the role of superconducting versus nonsuperconducting pinning centers. The third sample, Nb-up, was the reference which allows to study and compare the role of corrugation. In addition to these samples we grew the following reference samples: Nb film (40 nm), V film (100 nm), and Nb (40 nm)/V (100 nm) bilayer.

All samples were grown on 4×4 mm^2 highly resistive ($\rho = 5000-8000\,\Omega$ cm) (100) silicon substrates. V film, 100 nm thickness, was deposited simultaneously on all samples. Metal evaporation was done by electron beam deposition at a rate of 3 Å/s in a high-vacuum system with a base pressure of 2×10^{-8} Torr.

The coverage of large-area samples with Nb and Cu dots was achieved using 300-nm-thick Al$_2$O$_3$ porous membranes. These membranes were fabricated from pure (99.99%) Al foil following the two-step anodization method described in Ref. [21]. After anodization, the membranes were transferred onto Si substrates, for the fabrication of Nb-down and Cu-down, and onto V thin film for the Nb-up sample. The membrane transferring process was conducted following the method described elsewhere [22]. This approach allows obtaining nanopatterns in large areas and therefore enabling the characterization of magnetic properties by conventional magnetometry techniques.

Figure 1 shows the scanning electron microscopy (SEM) of the Nb array in the Nb-down sample, prior to V deposition. The thickness of Cu and Nb dots $t = 40$ nm was determined from low-angle x-ray reflectivity using continuous reference films. SEM characterization shows that Nb and Cu dots are arranged in triangular lattices with identical density and comparable domain size (larger than several microns). Dot diameter $d = 70$ nm ± 5 nm and lattice parameter $a = 100$ nm ± 5 nm were obtained by quantitative image analysis using the Microscopy Image Segmentation Tool (MIST) software [23].

Electrical transport and magnetization measurements were conducted in a Quantum Design Dynacool system. All temperature-dependent measurements were carried out following a zero-field cool protocol: The samples were cooled to 2 K at zero magnetic field before the measurements were initiated. In all cases, the applied magnetic field was perpendicular to the sample surface. Magnetization measurements were performed by vibrating sample magnetometry (VSM) as a function of field (± 5 T), and as a function of temperature (2−9 K). Subsequent magnetoresistance measurements were performed using a four-probe configuration with electrical currents in the range of 1 μA to 10 mA. The temperature was set with a pre-
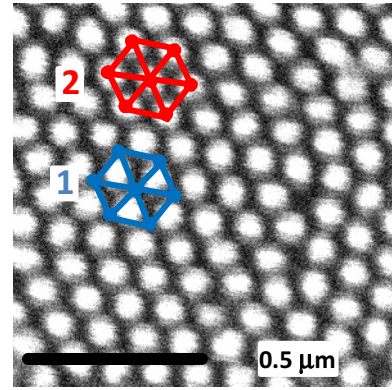
FIG. 1. (Color online) SEM image of triangular array of Nb dots grown on Si substrate. Drawn hexagons show two different locations for vortices in SC (1, blue line) and non-SC (2, red line) pinning centers.

cision of ± 1 mK. In addition to these standard measurements, the superconducting transition of Nb dots was independently determined from magnetic field modulated microwave spectroscopy (MFMMS) [24]. The MFMMS data were obtained with 200-Oe external dc field, which is modulated by a 15-Oe ac field at 100 kHz and 1 mW of microwave power.

III. RESULTS

The superconducting critical temperature (T_C) and transition width (ΔT_C) of Nb-down, Cu-down, Nb-up, and the three reference samples: Nb film (40 nm), V film (100 nm), and Nb (40 nm)/V (100 nm) bilayer (with V on the top of Nb), are shown in Table I. T_C values were obtained by resistive measurements, choosing a criterion of $0.8 R_N$, where R_N is the normal-state resistance. Nb-down and Cu-down samples show wider and multistep transitions, $\Delta T_C = 0.5$ and 0.4 K, and $T_C = 4.08$ and 4.33 K, respectively. Nb-up and the reference V film show the same $T_C = 4.77$ K and $\Delta T_C = 0.01$ K. The lower T_C and larger ΔT_C of the samples with underlying dots can be attributed to the presence of corrugation (film thickness variations) [25] and confinement effects [26]. Since the dot dimensions ($d = 70$ nm and $t = 40$ nm) are comparable to the Bardeen-Cooper-Schrieffer (BCS) coherence lengths— $\xi_{o,Nb} = 38$ nm [27] and $\xi_{o,V} = 44$ nm [28] for Nb and V,

TABLE I. Superconducting critical temperature (T_C) and transition width (ΔT_C) obtained by zero-field resistance measurements. The value of T_C was determined by $0.8 R_N$ criterion.

Sample	T_C (K)	ΔT_C (K)
Nb dots	6.10[a]	–
Nb film (40 nm)	8.00	0.01
V film (100 nm)	4.77	0.01
Nb/V bilayer	8.10	0.21
Nb-down	4.08	0.50
Cu-down	4.33	0.40
Nb-up	4.77	0.01

[a]T_C of Nb dots was obtained by MFMMS.
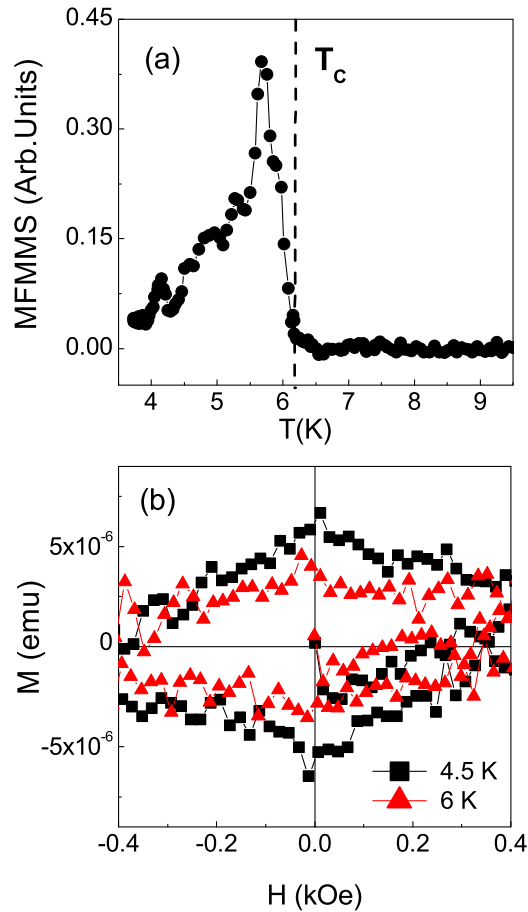
FIG. 2. (Color online) (a) MFMMS signal as a function of temperature with 200-Oe applied dc magnetic field for Nb dots (sample Nb-down before V film deposition). (b) $M(H)$ at 4.5 and 6 K for Nb-down (after V deposition).

respectively—it is expected that these two effects play an important role. Confinement can also weaken superconductivity in the thinner regions of the corrugated V film where vortex pinning may occur preferentially.

Nb-up and V-film reference sample have the same T_C which confirms that there is no strong proximity coupling between V film and Nb dots. This lack of interaction between Nb and V can be related to the appearance of an oxide layer which could be formed during the anodic aluminum oxide (AAO) membrane transfer process. Consequently, proximity effects between Nb dots and V film are neglected in this paper. In addition, the critical temperatures of Nb/V bilayer and Nb-film reference sample are very similar and therefore the superconductivity of Nb film is not significantly affected by the proximity with V in the Nb/V bilayer.

We measured the T_C of Nb dots by MFMMS at different magnetic fields before V-film deposition. This high-sensitivity technique allows detecting superconductivity in discontinuous systems. Figure 2(a) shows the temperature dependence of the MFMMS signal across the SC transition. In spite of the high microwave power absorption by the Si substrates, the SC transition peak of Nb nanodots appears as a peak [24] at 6.1 K. The result shown in Fig. 2(a) was obtained with 200-Oe dc field applied perpendicular to the sample surface.
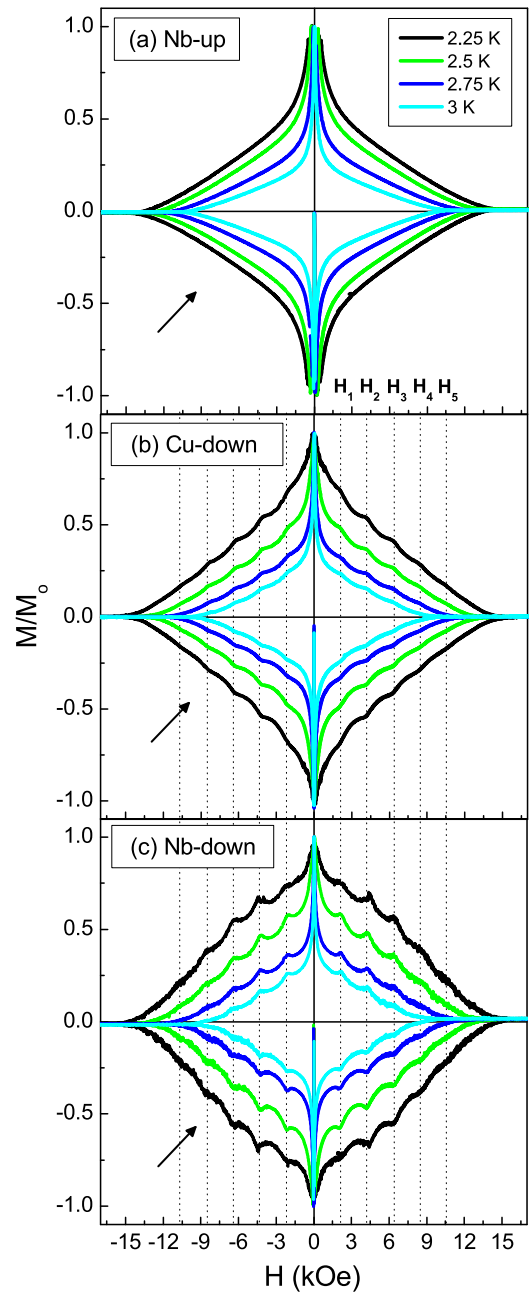
FIG. 3. (Color online) Superconducting loops normalized to maximum magnetization values at different temperatures for (a) Nb-up, (b) Cu-down, and (c) Nb-down. Dashed vertical lines highlight the matching fields at $M(H)$ maxima positions. Arrows point towards increasing temperatures.

No significant change of the SC transition temperature was observed for magnetic fields below 1000-Oe dc field. After the V film deposition on the Nb dots (sample Nb-down), we measured magnetization loops above the T_C of V, at 4.5 and 6 K. The $M(H)$ loops in Fig. 2(b) confirm the SC character of the Nb dots after V deposition. The rather low $T_C = 6.1$ K for the bare Nb dots lattice confirms the effect of finite size and lateral confinement in the sample.

Figure 3 shows the $M(H)$ loops normalized to maximum magnetization of the three samples below 3 K at the SC state. Prominent peaks up to fifth order can be observed for both Cu-down [Fig. 3(b)] and Nb-down [Fig. 3(c)] samples. These peaks precisely occur at the same field values for both samples. Furthermore, the periodicity of the peaks, $\Delta H = 2.12 \pm 0.02\,\text{kOe}$, correctly agrees with the matching field values expected for a similar triangular array of dots with a lattice parameter $a = 100 \pm 10\,\text{nm}$, $H_n = n\frac{2}{\sqrt{3}}\frac{\varnothing_0}{a^2} = n(2.39 \pm 0.48)\,\text{kOe}$, where $\varnothing_0 = 2.07 \times 10^{-15}$ Wb is the flux quantum, and n is the matching field order. This indicates that the vortex lattices in both samples, with SC and non-SC pinning centers, are commensurate to the pinning landscape at the same fields, i.e., to the lattice parameter determined by SEM. Note that the initial position of the vortices in relation to the pinning sites, either on vertices or interstitial, does not affect the lattice parameters, i.e., matching field values (see drawn hexagons in Fig. 1). It is also worth noting the lack of matching anomalies in the Nb-up sample which can be attributed to the absence of corrugation in the V film.

Figure 4 shows the normalized magnetoresistance $R(H)/R_N$ used to compare the pinning strength of all three samples close to T_C. Matching fields are observed in Cu-down [Fig. 4(b)] and Nb-down [Fig. 4(c)] samples at the same field values, which is consistent with magnetization data in Fig. 3. Nb-down shows pronounced minima up to the second order in a wide temperature range, from 3.83 to 4.10 K ($0.94T_C$ to $0.99T_C$), whereas Cu-down shows less pronounced minima only up to the first order in a narrower temperature range, from 3.95 to 4 K ($0.91T_C$ to $0.92T_C$). Furthermore, as expected from the magnetometry [Fig. 3(a)], no matching effects are observed for Nb-up [Fig. 4(a)].

In order to highlight important differences between the three samples, we compare the normalized resistances and magnetization at the same reduced temperature in Fig. 5. The normalized $M(H)/M_0$ superconducting loops at $T/T^* = 0.52$ for Nb-up, Nb down, Cu-down, and the Nb/V bilayer are shown in Fig. 5(a). The Nb-down sample shows stronger superconductivity, evidenced by sharper matching field peaks and larger loop width. We computed the normalized loop widths $\Delta M(H)/M_0$ from Fig. 5(a). These widths are proportional to the critical current density, $J_C(H)$, as stated by the Bean model [29]. At $T/T^* = 0.52\,\text{K}$, J_C of Nb-down, evaluated at the second matching field, shows a relative increase of $\sim$30% with respect to Cu-down, $\sim$120% with respect to Nb-up, and $\sim$190% with respect to Nb/V bilayer. Figure 5(b) shows $R(H)/R_N$ at $T/T^* = 0.92$ with T^* the onset of the superconducting transition for each sample. Close to T_C, the normalized resistance is higher for the Nb-down than the other two samples. Despite the superconducting character of the Nb dots, in this temperature range, the superconductivity of Nb-down weakens more with temperature than Cu-down.

In order to understand why the sample with superconducting pinning centers has higher critical current density at low temperature but higher resistance and lower critical temperature, we compared the temperature dependence of the critical fields and the normalized areas of the hysteresis loops of three samples. The inset of Fig. 6 compares the temperature dependence of the critical field (H_{C2}) calculated
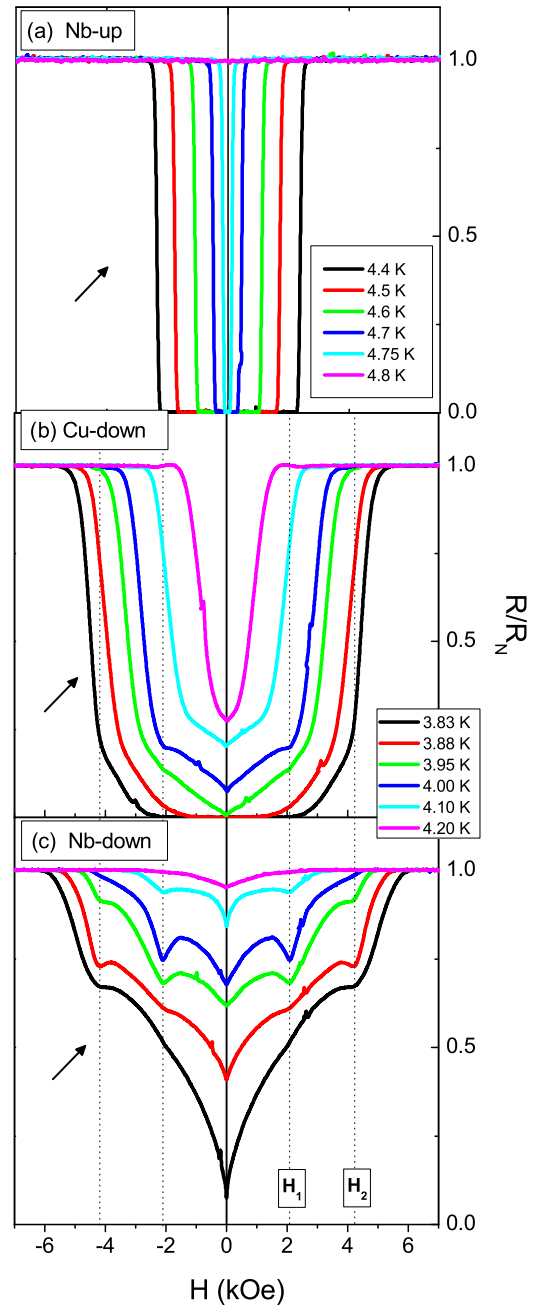
FIG. 4. (Color online) Magnetoresistance normalized to the resistance in the normal state at different temperatures for (a) Nb-up, (b) Cu-down, and (c) Nb-down samples. Dashed vertical lines highlight the matching fields as resistance minima. H_1 and H_2 indicate the first two matching fields. Arrows point towards increasing temperatures.

from the loops in Fig. 3 at $M(H) = 0$. Below $T = 3\,\text{K}$, H_{C2} of Nb-down is higher than Cu-down and Nb-up, while it is lower above $T = 3\,\text{K}$. Extrapolated H_{C2} ($T = 0\,\text{K}$) values are 36.4, 32.9, and 27.7 kOe for Nb-down, Cu-down, and Nb-up, respectively. Figure 6 shows the total area of M/M_o versus H cycles as a function of temperature for the three samples. These normalized hysteresis loop areas are also related to the critical currents since H_{C2} does not vary significantly between samples [see Fig. 5(a)]. The difference in critical current density of Nb-down and Cu-down decreases with temperature until they
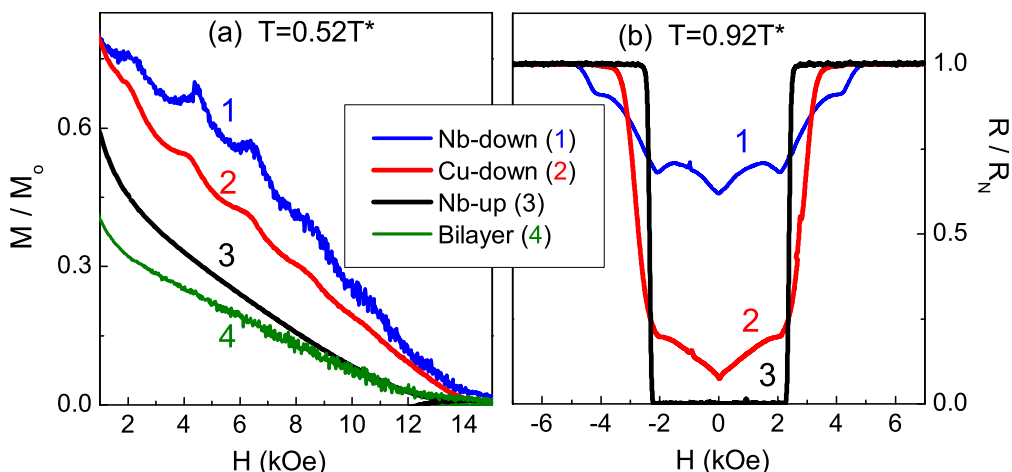
FIG. 5. (Color online) For Nb-down (1, blue line), Cu-down (2, red line), Nb-up (3, black line) and Nb/V bilayer (4, green line): (a) First quadrant of $M(H)$ loops normalized to maximum magnetization values at $T = 0.52T^*$ K. (b) Magnetoresistance normalized to the resistance in the normal state at $T = 0.92T^*$.

cross at $T \sim 3$ K. This result is consistent with the behavior of the critical field values for all samples.

IV. DISCUSSION

Although Nb-down has lower T_C than Cu-down and Nb-up, we can separate two different temperature regions in which the comparison between the other SC parameters changes gradually. At low temperatures, $T < 3$ K, the sample with SC pinning centers (Nb-down) shows more robust superconductivity characterized by sharper matching field peaks, higher critical fields, and larger critical currents (see Figs. 5 and 6). However, as temperature increases, the SC properties of V on the SC pinning centers (Nb-down) decrease faster, even though the Nb dots remain in the SC state. Above 3 K, Nb-down shows higher resistance, lower critical currents, and lower critical fields (see Figs. 5 and 6), although it shows well-defined resistive minima up to second order in an unusually wide temperature range [see Fig. 4(c)]. These minima occur at the
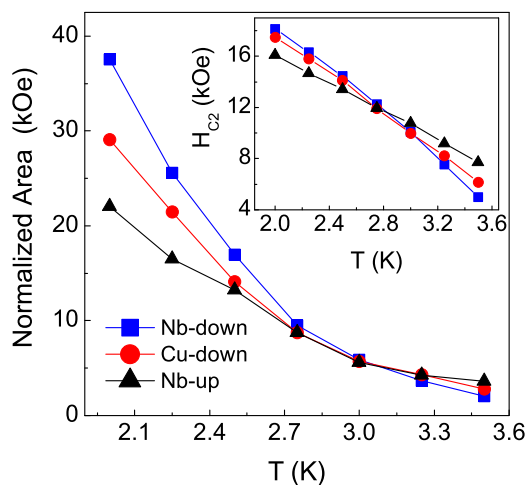
expected matching field values, consistent with magnetization data in Fig. 3.

This behavior cannot be attributed to better pinning in non-SC dots, since SC dots show sharper and higher-order resistive minima. We relate this contradictory behavior to a change in the nature of the resistance minima at 3 K. Previous pinning experiments show that when $\xi(T)$ becomes larger than the edge-to-edge distance between pinning centers (w), the nature of resistance minima changes. Minima are no longer related to commensurability of the vortex lattice and the pinning centers [30–32]. They arise from fluxoid quantization, which induces additional T_C suppression at noninteger flux quanta [33]. This behavior is known as the superconducting wire network regime.

For the three samples, $\xi(T) = (\frac{\emptyset_0}{2\pi H_{C2}(T)})^{1/2}$ was calculated from the temperature dependence of the upper critical field depicted in the inset of Fig. 6 for $T \leqslant 3.5$ K and from the upper critical field measured by transport for $T > 3.8$ K. In the latter, H_{C2} was defined at 80% of the normal-state resistance in the superconducting transition measured with different applied fields. Figure 7 shows the temperature dependence of $\xi(T)$ [$\xi(T) \sim \xi(0)(1 - T/T_C)^{-1/2}$] for the three samples. The extrapolated zero-temperature $\xi(0)$ are 9.52, 10, and 10.91 nm for Nb-down, Cu-down, and Nb-up, respectively. The horizontal dotted line in Fig. 7 indicates the temperature at which the vortex core diameter [$\sim 1.84 \times \xi(T)$] becomes comparable to the edge-to-edge separation between the dots ($w \sim 30$ nm). The crossover at which $1.84 \times \xi \sim w = 30$ nm coincides with the temperature where H_{C2} and J_C of Nb-down and Cu-down samples cross ($T \sim 3$ K).

In addition, one of the consequences of the SC network regime is the appearance of H_{C2} oscillations [16,17] with the same field period as that observed in the $R(H)$ curves. The inset of Fig. 7 shows the nonlinear temperature dependence of H_{C2} for Nb-down in which a peak at the first matching field, $H_1 = 2.08$ kOe, is superimposed. This curve suggests the change to a SC network regime near T_C.

It has been shown that in samples with non-SC pinning centers, vortices pin on top of the dots, and in interstitial

FIG. 6. (Color online) Temperature dependence of the normalized area of the hysteresis loops. Inset: Temperature dependence of H_{C2} obtained from loops in Fig. 3.

FIG. 7. (Color online) Temperature dependence of coherence length for Nb-down (blue squares), Cu-down (red circles), and Nb-up (black triangles). Inset: Temperature dependence of H_{C2} for Nb-down.

fluxoids spread over several dot lattice cells. This vortex regime change explains the overall increase in the resistance and the crossover in the temperature dependence of the critical field and critical current of Nb-down and Cu-down samples at $T = 3$ K.

The previous argument also explains the lack of pinning in samples without corrugation, i.e., Nb-up sample. Corrugation is still the main pinning mechanism, while the repulsive forces between the diamagnetism of the pinning centers and the vortices strengthens the pinning at low temperature, but it is not enough to lock the vortex lattice by itself.

However, further studies on the interaction between vortices and pinning centers across the transition to the SC wire network regime are necessary to support the conclusions. In order to obtain more information on the processes behind the observed decrease of the SC thin film properties, we suggest that a study of this process using different dot widths and lattice parameters is required. Ideally one would choose two materials that fulfill $T_{C,\text{dots}} > T_{C,\text{film}}$ and $H_{C2,\text{dots}} < H_{C2,\text{film}}$. This system would allow tuning the SC state of the dots by applying an external field, while the film is in the wire network regime. If superconductivity of the dots is related to the decrease of the superconducting properties of the thin film, a sudden improvement of them is expected when the dots become a normal metal.

V. CONCLUSIONS

We presented a systematic study on the role of superconducting pinning centers and corrugation on the pinning in the superconducting film. The corrugation decreases the critical temperature of the film, but it is necessary for pinning. SC pinning centers strengthen the pinning, increasing the sharpness and depth of resistance minima and the width of magnetization loops at low temperatures (below 3 K). However, these behaviors show unexpected temperature dependence and the presence of SC pinning centers induces a faster decrease of the SC properties above 3 K. The V thin film ($T_C \sim 4.5$ K) with Nb pinning centers ($T_C \sim 6.1$ K) has a higher resistance, lower critical field, lower critical temperature, and lower critical current than a V thin film with Cu pinning centers. This effect is related to a change in the nature of the resistance minima when the edge-to-edge distance between pinning centers is of the order of the vortex core diameter.

positions depending on the external applied magnetic field. When the applied field reaches $H = H_s = n_s H_1$, where n_s is the "saturation number," an additional flux line penetrating the film will be repelled into the interstitial region between the dots [34]. Interstitial vortices are only stable due to caging between vortices [6,35]. On the contrary, it is accepted [18] that SC pinning centers pin vortices in interstitial positions. This is due to the diamagnetic repulsion between vortices and SC pinning sites. Based on these results, we assume that in Cu-down, vortices pin on top of the attractive pinning centers and in interstitial positions. Note that for $T < 3$ K, $n_s = \frac{d}{4\xi(T)} \sim 1$ and the maximum number of vortices per pinning center derived from Fig. 3 is $n_{\max} = 5$. In Nb-down, the vortices pin preferentially in interstitial positions. SEM images of samples similar to the ones described here indicate that the superconducting layer on top of the nanodots is thinner between dots and thicker on top of the dots. In addition the low ratio $a/d \sim 1$ corresponds to the case of thin superconducting interstices of width $a - d \sim \xi_o$ [36]. These results support our point; corrugation and confinement effects weaken the superconductivity in interstitial positions. Therefore these regions act as preferential pinning centers. At low temperatures, the repulsive interactions exerted by the SC pinning sites assist pinning by caging the vortices at interstitial positions. However, at higher temperatures, the interaction between SC pinning sites and flux lines weaken the superconductivity when the superconducting regime changes from pinning enhancement to SC wire network in which

---

[1] A. I. Larkin and Yu. N. Ovchinnikov, J. Low Temp. Phys. **34**, 409 (1979).

[2] A. Hoffmann, P. Prieto, and I. K. Schuller, Phys. Rev. B **61**, 6958 (2000).

[3] C. Reichhardt and C. J. Olson Reichhardt, Phys. Rev. B **76**, 094512 (2007).

[4] S. Guénon, Y. J. Rosen, Ali C. Basaran, and I. K. Schuller, Appl. Phys. Lett. **102**, 252602 (2013); D. Ray, C. J. Olson Reichhardt, B. Jankó, and C. Reichhardt, Phys. Rev. Lett. **110**, 267001 (2013).

[5] A. T. Fiory, A. F. Hebard, and S. Somekh, Appl. Phys. Lett. **32**, 73 (1978).

[6] K. Harada, O. Kamimura, H. Kasai, T. Matsuda, A. Tonomura, and V. V. Moshchalkov, Science **274**, 1167 (1996).

[7] V. Metlushko, U. Welp, G. W. Crabtree, R. Osgood, S. D. Bader, L. E. DeLong, Z. Zhang, S. R. J. Brueck, B. Ilic, K. Chung, and P. J. Hesketh, Phys. Rev. B **60**, R12585 (1999).

[8] G. R. Berdiyorov, M. V. Milošević, and F. M. Peeters, Phys. Rev. Lett. **96**, 207001 (2006); Phys. Rev. B **74**, 174512 (2006).

[9] A. Bezryadin, Yu. N. Ovchinnikov, and B. Pannetier, Phys. Rev. B **53**, 8553 (1996).

[10] S. Raedts, A. V. Silhanek, M. J. Van Bael, and V. V. Moshchalkov, Phys. Rev. B **70**, 024509 (2004).

[11] J. I. Martín, M. Vélez, J. Nogués, and I. K. Schuller, Phys. Rev. Lett. **79**, 1929 (1997).

[12] M. Lange, M. J. Van Bael, Y. Bruynseraede, and V. V. Moshchalkov, Phys. Rev. Lett. **90**, 197006 (2003); M. V. Milošević and F. M. Peeters, Europhys. Lett. **70**, 670 (2005).

[13] Y. Jaccard, J. I. Martín, M.-C. Cyrille, M. Vélez, J. L. Vicent, and I. K. Schuller, Phys. Rev. B **58**, 8232 (1998).

[14] M. J. Van Bael, K. Temst, V. V. Moshchalkov, and Y. Bruynseraede, Phys. Rev. B **59**, 14674 (1999).

[15] X. S. Ling, H. J. Lezec, M. J. Higgins, J. S. Tsai, J. Fujita, H. Numata, Y. Nakamura, Y. Ochiai, Chao Tang, P. M. Chaikin, and S. Bhattacharya, Phys. Rev. Lett. **76**, 2989 (1996).

[16] R. D. Parks and W. A. Little, Phys. Rev. **133**, A97 (1964)

[17] B. Pannetier, J. Chaussy, R. Rammal, and J. C. Villegier, Phys. Rev. Lett. **53**, 1845 (1984).

[18] G. R. Berdiyorov, V. R. Misko, M. V. Milošević, W. Escoffier, I. V. Grigorieva, and F. M. Peeters, Phys. Rev. B **77**, 024526 (2008).

[19] J. I. Facio, A. Abate, J. Guimpel, and P. S. Cornaglia, J. Phys.: Condens. Matter **25**, 245701 (2013).

[20] S. J. Carreira, C. Chiliotte, V. Bekeris, Y. J. Rosen, C. Monton, and I. K. Schuller, Supercond. Sci. Technol. **27**, 085007 (2014).

[21] C.-P. Li, I. V. Roshchin, X. Batlle, M. Viret, F. Ott, and I. K. Schuller, J. Appl. Phys. **100**, 074318 (2006).

[22] J. E. Allen, K. G. Yager, H. Hlaing, C. Y. Nam, B. M. Ocko, and C. T. Black, Appl. Phys. Lett. **99**, 163301 (2011).

[23] I. Valmianski, C. Monton, and I. K. Schuller, Rev. Sci. Instrum. **85**, 033701 (2014).

[24] J. G. Ramírez, A. C. Basaran, J. de la Venta, J. Pereiro, and I. K. Schuller, Rep. Prog. Phys. **77**, 093902 (2014).

[25] M. I. Montero, J. J. Akerman, A. Varilci, and I. K. Schuller, Europhys. Lett. **63**, 118 (2003).

[26] S. Bose, P. Raychaudhuri, R. Banerjee, P. Vasa, and P. Ayyub, Phys. Rev. Lett. **95**, 147003 (2005).

[27] C. Kittel, *Introduction to Solid State Physics*, 7th ed. (Wiley, New York, 1996).

[28] I. A. Garifullin, N. N. Garif'yanov, R. I. Salikhov, and L. R. Tagirov, JETP Lett. **87**, 316 (2008).

[29] C. P. Bean, Phys. Rev. Lett. **8**, 250 (1962); Rev. Mod. Phys. **36**, 31 (1964).

[30] U. Patel, Z. L. Xiao, J. Hua, T. Xu, D. Rosenmann, V. Novosad, J. Pearson, U. Welp, W. K. Kwok, and G. W. Crabtree, Phys. Rev. B **76**, 020508(R) (2007).

[31] V. V. Moshchalkov, M. Baert, V. V. Metlushko, E. Rosseel, M. J. Van Bael, K. Temst, Y. Bruynseraede, and R. Jonckheere, Phys. Rev. B **57**, 3615 (1998).

[32] U. Welp, Z. L. Xiao, J. S. Jiang, V. K. Vlasko-Vlasov, S. D. Bader, G. W. Crabtree, J. Liang, H. Chik, and J. M. Xu, Phys. Rev. B **66**, 212507 (2002).

[33] M. Tinkham, D. W. Abraham, and C. J. Lobb, Phys. Rev. B **28**, 6578 (1983).

[34] V. V. Metlushko, L. E. DeLong, V. V. Moshchalkov, and Y. Bruynseraede, Physica C **391**, 196 (2003).

[35] C. Reichhardt and C. J. Olson Reichhardt, Phys. Rev. B **79**, 134501 (2009).

[36] L. E. De Long, S. Kryukov, V. V. Metlushko, V. V. Moshchalkov, and Y. Bruynseraede, Physica C **404**, 123 (2004).